Available online at www.sciencedirect.com
ScienceDirect
Journal of Non-Crystalline Solids 353 (2007) 2307–2317
JOURNAL OF NON-CRYSTALLINE SOLIDS
www.elsevier.com/locate/jnoncrysol

Surface and bulk residual stresses in $Li_2O \cdot 2SiO_2$ glass–ceramics

H. Pinto [a,b,*], L. Ito [a,c], M. Crovace [a,c], E.B. Ferreira [c], F. Fauth [d], T. Wroblewski [e], E.D. Zanotto [c], A.R. Pyzalla [a,b]

[a] *Institute of Materials Science and Material Technology, TU Wien, Karlsplatz 13, 1040 Vienna, Austria*
[b] *Max-Planck-Institut für Eisenforschung GmbH, Max-Planck-Strasse 1, 40237 Düsseldorf, Germany*
[c] *Vitreous Materials Laboratory (LaMaV), Department of Materials Engineering (DEMa), Federal University of Sao Carlos (UFSCar), CEP 13565-905, São Carlos, SP, Brazil*
[d] *European Synchrotron Radiation Facility (ESRF), BP 220, 38043 Grenoble, France*
[e] *HASYLAB at DESY, Notkestrasse 85, D-22607 Hamburg, Germany*

Received 11 July 2006; received in revised form 16 April 2007

Abstract

In the present work surface and bulk residual stresses generated in partially crystallized $Li_2O \cdot 2SiO_2$ glass–ceramics are analyzed after different heat treatments. The phase specific residual stresses in the crystalline $Li_2Si_2O_5$-phase are evaluated for the first time in the near-surface zone and the bulk of the samples using both medium and high energy synchrotron radiation. The results reveal that in the crystals within the bulk of the samples micro residual stresses generated by the thermal anisotropy of the isolated individual crystallites depend on the crystallographic direction. In contrast, the residual stress state in the near-surface zone is isotropic due to the superposition of thermal residual stresses in and around the crystals of the near-surface area. Residual stress calculations using a modified Selsing's model yield a good estimate of the anisotropic residual stresses in the bulk crystallites, whereas the isotropic residual stress state in the crystallized surface layer can be described by an elastic stress model for thin films.
© 2007 Elsevier B.V. All rights reserved.

PACS: 81.05.Pj; 81.40.−z; 81.40.Jj; 61.10.Nz

Keywords: Glass–ceramics; Synchrotron radiation; Anisotropy; Residual stresses; Microstructure

1. Introduction

Glass–ceramics are polycrystalline solids manufactured by controlled crystallization of glasses. Usually the glass is quenched from the melt, shaped and subsequently converted into a glass–ceramic by an appropriate heat treatment above the glass transition temperature T_g. Glass–ceramics are typically pore-free, their microstructure can be well controlled, and components with complex shapes can be manufactured. Among their manifold applications are components for domestic use, e.g. kitchenware and hot plates, but also artificial teeth, bones, and telescope mirrors. However, the application of glass–ceramics might be limited by inadequate mechanical properties [1]. Their mechanical performance is not only determined by the microstructure (crystallite size, shape and orientation, crystallized volume fraction, etc.), but also by the residual stresses [2].

The residual stress state within a glass–ceramic component consists of a superposition of macro and micro residual stresses [3]. Macro residual stresses, referred also as thermal tempering stresses [4,5], result from temperature

* Corresponding author. Address: Max-Planck-Institut für Eisenforschung GmbH, Max-Planck-Strasse 1, 40237 Düsseldorf, Germany. Tel.: +49 211 6792 400; fax: +49 211 6792 390.
E-mail address: h.pinto@mpie.de (H. Pinto).

0022-3093/$ - see front matter © 2007 Elsevier B.V. All rights reserved.
doi:10.1016/j.jnoncrysol.2007.04.007

gradients during manufacturing. They can be minimized by slow and homogeneous cooling and/or subsequent annealing of the component [6]. Micro residual stresses result from strains originating from density changes introduced by the crystallization process [7,8] and from strains caused by differences in the thermal and elastic properties of the crystalline and the amorphous phase during cooling down to room temperature [9,10]. The micro stresses generated during crystal nucleation relax by viscous flow, if crystallization occurs above T_g. Additional micro residual stresses arise in the near-surface zone of glasses due to the crystallization of surface layers. Macro and micro residual stresses in the bulk material as well as in the near-surface zone strongly influence crack nucleation and propagation processes [2] and may, thus, affect the functionality, reliability, and lifetime of glass–ceramics.

In the present work $Li_2O \cdot 2SiO_2$ glass–ceramic was chosen due to its technological importance. The possibility of achieving high mechanical strength makes these glass–ceramics suitable for e.g. substrates of computer hard discs. This system has been studied for several years, e.g. [11], and the accumulated knowledge allows a precise control of the microstructures by adequate heat treatments.

In case of $Li_2O \cdot 2SiO_2$ glass–ceramics the linear thermal expansion coefficients (α) experimentally determined in glassy and fully crystallized samples [12] revealed that α_g (glass) is larger than the average α_c (crystal). Therefore, residual stress calculations based on elastic models with spherical isotropic crystals show along the radial direction compressive micro stresses in the crystallites and balancing tensile micro stresses in the amorphous matrix. Experimental studies by X-ray diffraction [12], however, indicated tensile residual stresses in some crystallographic directions of the crystalline particles.

These tensile micro residual stresses might be due to a local anisotropy of the residual stress field originating from the low symmetry crystal structure (monoclinic with orthorhombic pseudo-symmetry [13]) of the $Li_2O \cdot 2SiO_2(LS_2)$ phase. In addition, spatial inhomogeneities might also arise due to the superposition of residual stress fields around neighboring crystallites [14]. Thus, e.g. gradients in the crystallized volume fraction across a sample cross-section supposedly affect the residual stresses in the crystalline phase of a glass–ceramic.

The aim of the present investigation is to contribute to the understanding of the residual stress state, particularly the residual micro stress state, in glass–ceramics. The focus is on determining the effects of the microstructure on the spatial inhomogeneity and local anisotropy of the residual stress field.

The residual stress state near the surface and in the bulk of $Li_2O \cdot 2SiO_2$ glass–ceramic samples obtained by two different heat treatments and, thus, containing different crystallized volume fractions is characterized using synchrotron radiation. The link between microstructure and the residual stress state is established by scanning electron microscopy.

2. Review of methods for residual stress analysis

2.1. Residual stress analysis in the bulk of the sample (3D residual stress state) [15,16]

In experimental stress analyses by X-ray and neutron diffraction, the crystal lattice strain $\varepsilon_{\varphi\psi}$ measured in the sample direction defined by the azimuthal φ and the tilting ψ angles (Fig. 1) with respect to the laboratory frame of reference is determined from the relative change in lattice distance due to applied or residual stresses, Eq. (1).

$$\varepsilon_{\varphi\psi} = \frac{(d_{\varphi\psi} - d_0)}{d_0} \tag{1}$$

$d_{\varphi\psi}$ is the lattice spacing measured and d_0 is the stress-free lattice spacing.

In the bulk of samples and components the residual stress state is usually triaxial. Therefore, in order to access the complete strain/stress tensor within the samples, measurements have to be performed in at least six specimen directions. In those cases, where measurements are performed in the directions of the principal stresses (in case these are known a priori), only three principal strains need to be determined in order to evaluate the principal stresses.

The residual stresses are calculated from the lattice strains using Hooke's law, Eq. (2).

$$\sigma_{ij} = \frac{1}{1/2S_2^{hkl}}\left[\varepsilon_{ij} - \left\{\delta_{ij}\frac{S_1^{hkl}}{1/2S_2^{hkl} + 3 \cdot S_1^{hkl}}\right\}(\varepsilon_{11} + \varepsilon_{22} + \varepsilon_{33})\right] \tag{2}$$

S_1^{hkl} and $1/2S_2^{hkl}$ are the diffraction elastic constants (DEC), δ is the Kronecker delta-function and ε_{11}, ε_{22} and ε_{33} are lattice strains measured along the principal axes of the stress tensor.

The evaluation of a triaxial (3D) stress state requires an accurate d_0-value (see Eq. (1)). The determination of the stress-free lattice spacing d_0 is often problematic [17]. Typical approximations for determining d_0 are lattice parameter measurements on powders, filings and small component

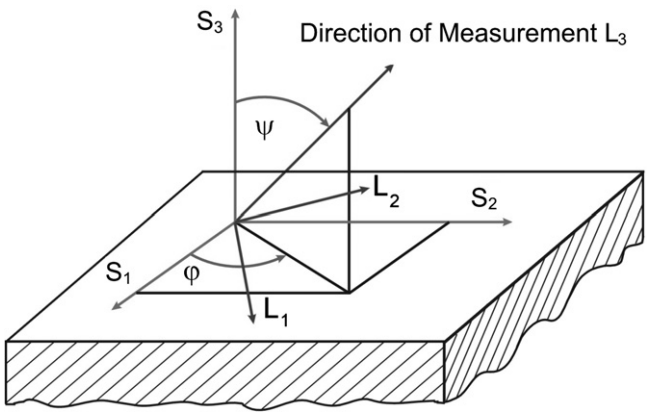

Fig. 1. Orientation angles φ and ψ, sample (S_i) and laboratory (L_i) frames of reference.

pieces or a calculation of d_0 based on mechanical equilibrium conditions.

2.2. Residual stress analyses in the near-surface zone (2D residual stress state)

In the near-surface zone, where due to stress balancing conditions the residual stress component perpendicular to the sample surface can be neglected, the $\sin^2\psi$-method is the traditional technique for residual stress analyses by X-ray diffraction [15,16,18,19]. If the principal directions of the residual stress state are known, the fundamental diffraction strain relationship can be expressed by

$$\varepsilon_{\varphi\psi} = \frac{d_{\varphi\psi} - d_0}{d_0} = 1/2S_{2(hkl)}\sigma_\varphi \sin^2\psi + S_{1(hkl)}(\sigma_{11} + \sigma_{22}) \quad (3)$$

$\varepsilon_{\varphi\psi}$ is the strain along the sample direction given by the azimuthal angle φ and the tilting angle ψ [see e.g. 16]. The slope of the experimentally determined d versus $\sin^2\psi$ curves is proportional to the stress σ_φ.

In case of an uniaxial or biaxial stress state, an accurate value of d_0 is not necessary to determine the stress σ_φ. Any uncertainty in d_0, which is usually easily determinable to a fraction of one percent, is only reflected to the same proportion in the uncertainty in stress and thus generally negligible in comparison to other uncertainties [19]. The principal stress components σ_{11} and σ_{22} are then evaluated from the slope of the $\varepsilon_{\varphi\psi}$ versus $\sin^2\psi$-curve for measurements at different azimuthal angles, e.g. $\varphi = 0°$ and 90°.

3. Experimental details

3.1. Sample preparation

A $Li_2O \cdot 2SiO_2$ glass of stoichiometric composition (33.3 mol% Li_2O) was prepared by melting a homogeneous mixture of reagent-grade Li_2CO_3 and SiO_2 in an electric furnace at 1450 °C for 3 h in a Pt crucible in air. The melt was cast into a cylindrical graphite mould (8 mm × 40 mm) at room temperature, and the glass was frozen with an estimated cooling rate of 400 °C/min. The glass cylinders were annealed at 444 °C ($T_g - 10$ °C) for 2 h and then cooled inside the furnace at a rate of about 1 °C/min in order to minimize temperature gradients across the sample diameter.

In order to obtain partially crystallized glasses, as-received cylindrical specimens 8 mm × 10 mm were subjected to isothermal heat treatments at 464 °C ($T_g + 10$ °C) for two different periods: 87 h and 96 h. The heat treatments were carried out in an electric furnace with a temperature control within ±1 °C. Afterwards, the specimens were clad and slowly cooled down in air. A fully crystallized sample with an average crystal diameter of 20 μm was obtained by nucleating crystals at 454 °C (T_g) for 24 h and then annealing at 600 °C for 20 min to allow for crystal growth.

3.2. Microstructure characterization

3.2.1. Microscopy

Polished glass–ceramic samples were etched in a diluted solution of HF/HCl (0.08/0.04 vol.%) for 1 min, and characterized using scanning electron microscopy (SEM). The very low crystalline volume fraction in the bulk material was quantitatively evaluated by analyzing several SEM micrographs using the UTHSCSA Image Tool (version 3.00) [20].

3.2.2. X-ray diffraction (XRD)

In order to determine the structure and volume fraction of the crystalline phase formed in the near surface zone and in the interior of the samples, synchrotron X-ray diffraction experiments were performed at the experimental station G3 of HASYLAB at DESY, Hamburg, Germany, using a radiation energy of 8.05 keV and a beam size of 2 × 2 mm^2. The diffractograms were analyzed by a Rietveld refinement procedure using the software MAUD (material analysis using diffraction) [21–25]. The instrument broadening function was determined using a standard silicon powder with a well-known grain size distribution. In order to evaluate the texture strength in the crystallized surface layer of the samples pole figures of the (111), (200), (002), and (170) lattice planes of the $Li_2Si_2O_5$-phase were measured using a laboratory X-ray source (Co–Kα-radiation).

3.3. Residual stress analysis

Analyses of the near-surface residual stresses by X-ray diffraction were carried out at the experimental station G3 of HASYLAB at DESY, Hamburg, Germany, using a radiation energy of 8.05 keV. The (110), (130), (040), (111), (200), (002), (330), (351), (281), (0100), (332), and (370) reflections of the $Li_2Si_2O_5$ phase were chosen for residual stress analysis by the $\sin^2\psi$-method. The ψ-angle ranged between 0° and 63° ($\sin^2\psi = 0.79$), step size $\Delta\sin^2\psi = 0.085$. Since there is no data available on the stiffnesses c_{ij} of the $Li_2Si_2O_5$ phase, its diffraction elastic constants (DEC) were approximated by the macroscopic Young modulus, E, and Poisson ratio, υ [12].

For triaxial residual stress analyses high energy synchrotron X-ray diffraction (HESD) experiments in transmission mode were performed at the European Synchrotron Radiation Facility (ESRF), Grenoble, France, at the beamline ID 31 using photons of 31.04 keV energy. The gauge volume was defined by slits in the incoming and the diffracted beam (0.5 × 2 mm^2). The gauge volume shape is similar to an elongated diamond with a volume of about 13 mm^3. The positions of the sample edges were defined by measurements of the transmitted total intensity through the sample versus sample translation in three directions.

A cylindrical system of principal stresses was assumed due to the cylindrical shape of the specimens. Thus, measurements were performed at (φ, ψ): (0, 0), (0, 90), and (90, 90), which correspond to the axial, radial and circumferential

directions of the cylindrical samples, respectively. For residual stress analyses the (1 1 0), (2 0 0), (0 0 2), (0 4 0), and (3 3 0) reflections were selected, since these lattice planes exhibit the highest thermal expansion mismatches ($\Delta\alpha$) with respect to the glass matrix (see [12]). The fully crystallized sample was milled down to about 5 μm grain size and the powder was used to estimate the d_0-value. The residual stresses were evaluated in five different gauge volumes centered on the mid-plane and equally distributed on the sample cross-section.

4. Results

4.1. Microstructure characterization

4.1.1. Microscopy

After both treatments (87 h and 96 h at 464 °C), a population of nearly spherical crystals of about 0.3 μm diameter was observed in the bulk of the samples (Fig. 2). Crystal branching, reported for specimens heat treated under more stringent conditions (502 h at 454 °C) [26], was not observed. The crystallized fraction in the bulk amounted to about 4% for the sample heat treated for 87 h and 7% for the sample heat treated for 96 h.

After the heat treatments, a fully crystallized layer of ~2.0–3.5 μm in thickness was visible (Fig. 3) at the surface of the specimens. Within this surface layer a morphological preferential orientation of crystal growth is apparent. Needle-shaped crystallites grow towards the bulk material, starting at the sample surface. An abrupt change in crystallinity occurs at the interface bulk material/fully crystallized surface layer, besides that no gradient of crystallinity is observed across the sample.

4.1.2. X-ray diffraction

Diffractograms obtained from the interior of the samples heat treated at 464 °C for 87 h and 96 h (Fig. 4) using high energy synchrotron diffraction (HESD) reveal only weak diffraction of the crystalline phase on a huge background resulting from the amorphous matrix (this precluded a

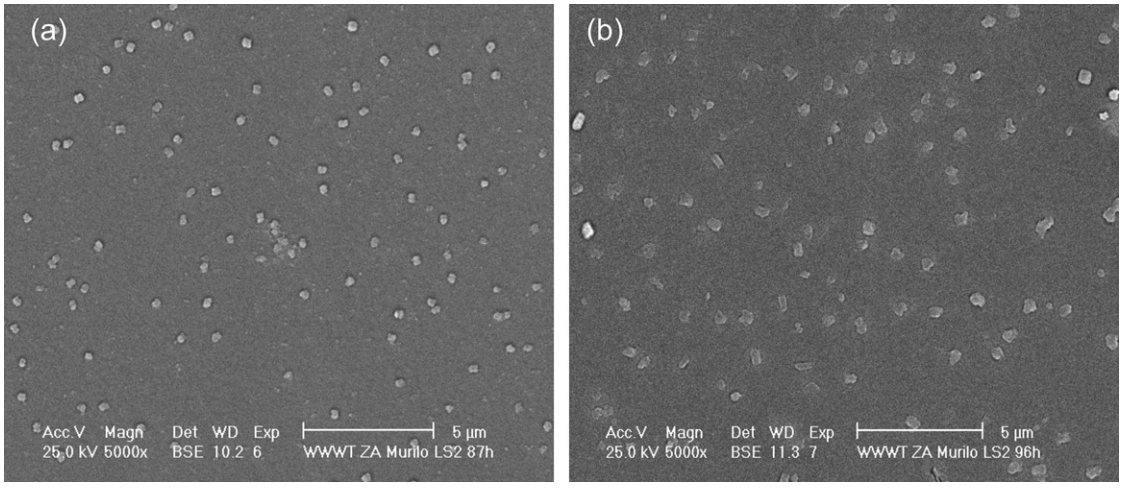

Fig. 2. SEM micrographs of bulk microstructures in specimens heat treated at 464 °C for 87 (a) and 96 h (b).

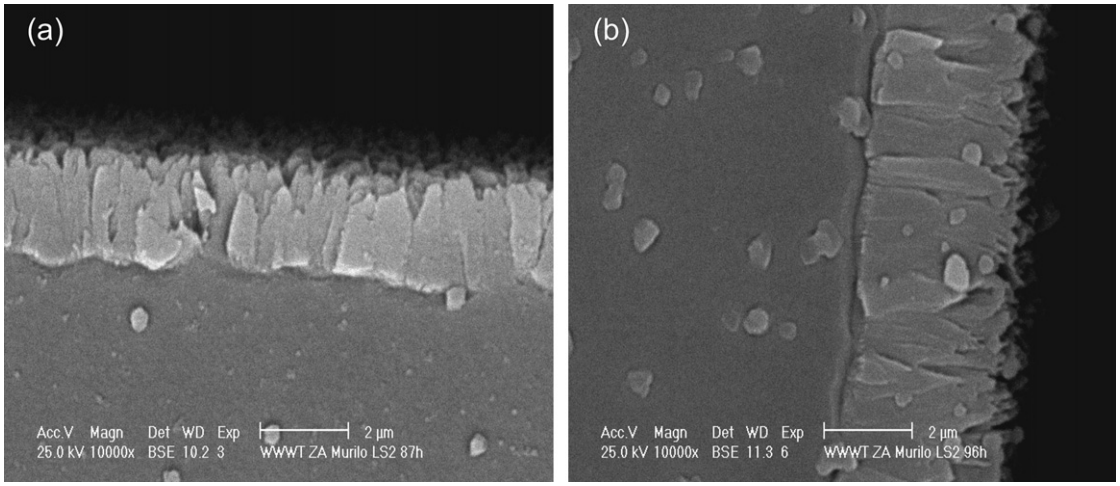

Fig. 3. SEM micrographs of the near-surface zone after heat treatment at 464 °C for 87 (a) and 96 h (b).

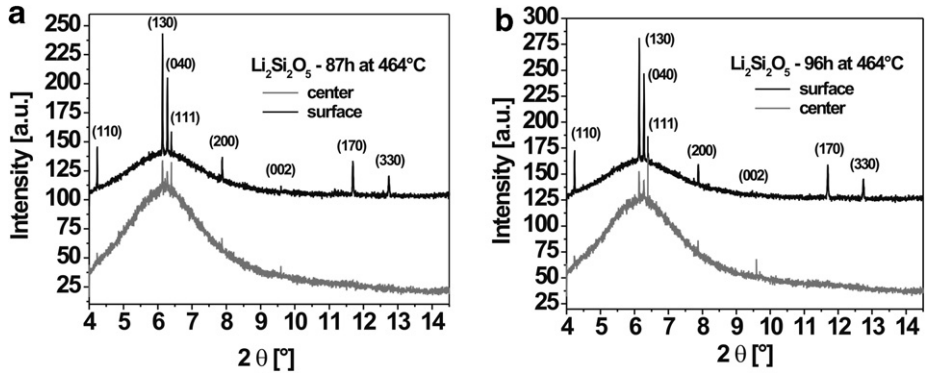

Fig. 4. Diffractograms from the sample center and surface recorded after both heat treatments using HESR: (a) 87 h, (b) 96 h.

quantitative phase analyses). The reflection profiles of both samples (heat treated for 87 h and 96 h) are similar.

In contrast to the low crystallinity in the bulk material, a significant volume fraction of crystallites in the near sample surface as well as in the fully crystallized sample yield well developed diffractograms (Figs. 4–7). According to [28,29],

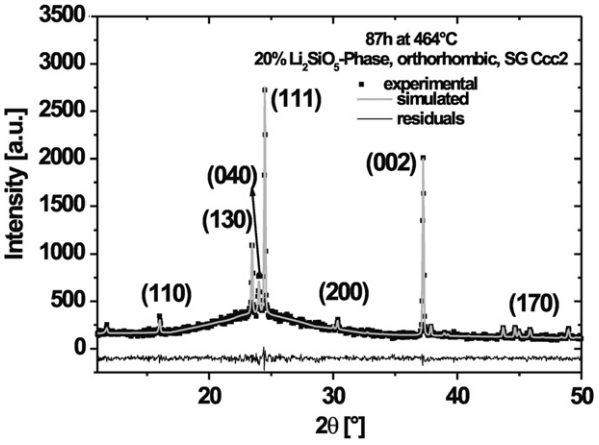

Fig. 5. Experimental and simulated diffraction patterns of the near-surface zone after heat treatment of 87 h at 464 °C.

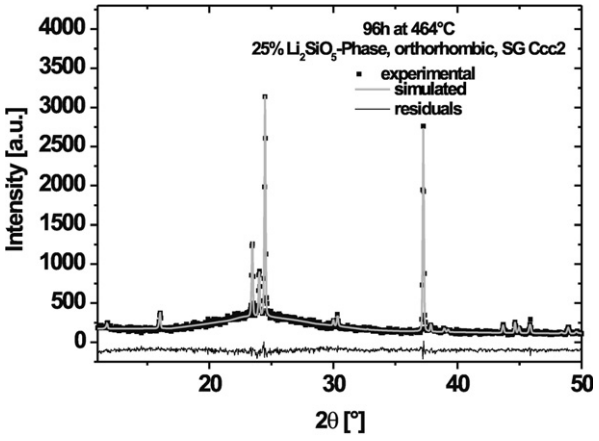

Fig. 6. Experimental and simulated diffraction patterns of the near-surface zone after heat treatment of 96 h at 464 °C.

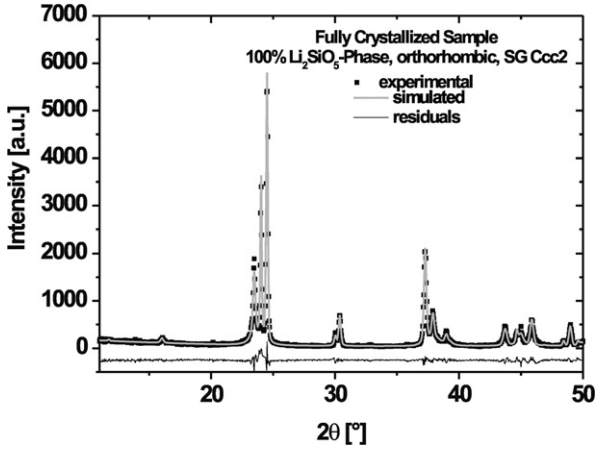

Fig. 7. Experimental and simulated diffraction patterns of the fully crystallized sample.

two crystalline lithium silicate phases (LS, LS_2) may be formed by heat treatments of $Li_2O \cdot 2SiO_2$ at 464 °C. LS is the metastable Li_2SiO_3-phase (orthorhombic, space group $Cmc2_1$, $a = 0.939$ nm, $b = 0.54$ nm, $c = 0.466$ nm, $\alpha = \beta = \gamma = 90°$) [31]. The LS_2 phase ($Li_2Si_2O_5$) has an orthorhombic crystal structure, space group Ccc2 ($a = 0.581$ nm, $b = 1.458$ nm, $c = 0.477$ nm, $\alpha = \beta = \gamma = 90°$), and is known to be the stable phase [13,30]. Rietveld refinements revealed that only $Li_2Si_2O_5$ crystallites are present in the samples (Figs. 5–7).

X-ray pole figures obtained from the near-surface zone of the fully crystallized sample (Fig. 8) revealed a weak (0 0 2) fiber component. This texture corresponds to a preferred orientation of the orthorhombic *c*-axis perpendicular to the sample surface within the surface layer.

4.2. Residual stress analysis

The phase specific residual stresses determined by HESD using several reflections of $Li_2Si_2O_5$-phase along all three sample directions are shown for the samples heat treated for 87 h and 96 h in Figs. 9 and 10, respectively.

The two gauge volumes at distances between ±4 mm from the center of the sample comprise the fully crystallized

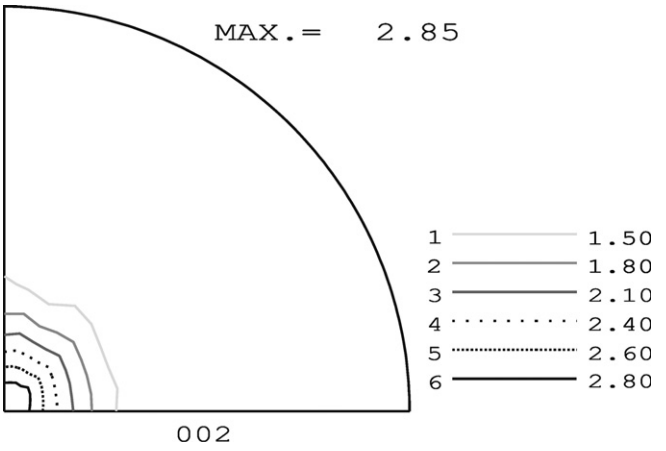

Fig. 8. Pole figure of the (002) lattice plane from the $Li_2Si_2O_5$-phase in a fully crystallized sample.

surface zone and the bulk microstructure. Due to the low crystalline volume fraction and the nanometric crystal size, the bulk microstructure yields only broad reflections with low peak-to-background ratio (Fig. 4). Thus, in the gauge volumes comprising the near-surface zone the intensity, the 2θ-position of the reflections and, consequently, the residual stress values obtained are influenced by the fully crystallized surface layer of the samples.

The three gauge volumes confined to distances between ± 2 mm from the sample center represent only bulk material. Thus, the intensity of the reflections obtained in these three gauge volumes is substantially lower than those obtained in the gauge volumes comprising the near-surface zone of the sample (Fig. 4). The residual stress values shown in Figs. 9 and 10 represent the phase specific residual stresses in the $Li_2Si_2O_5$ crystals determined in the direction of the principal stress components (radial, circumferential, and axial direction of the cylindrical samples) in the bulk of the samples.

In all analyzed gauge volumes the residual stress values of each single lattice plane are not significantly different in the different principal directions of the samples. Thus, the

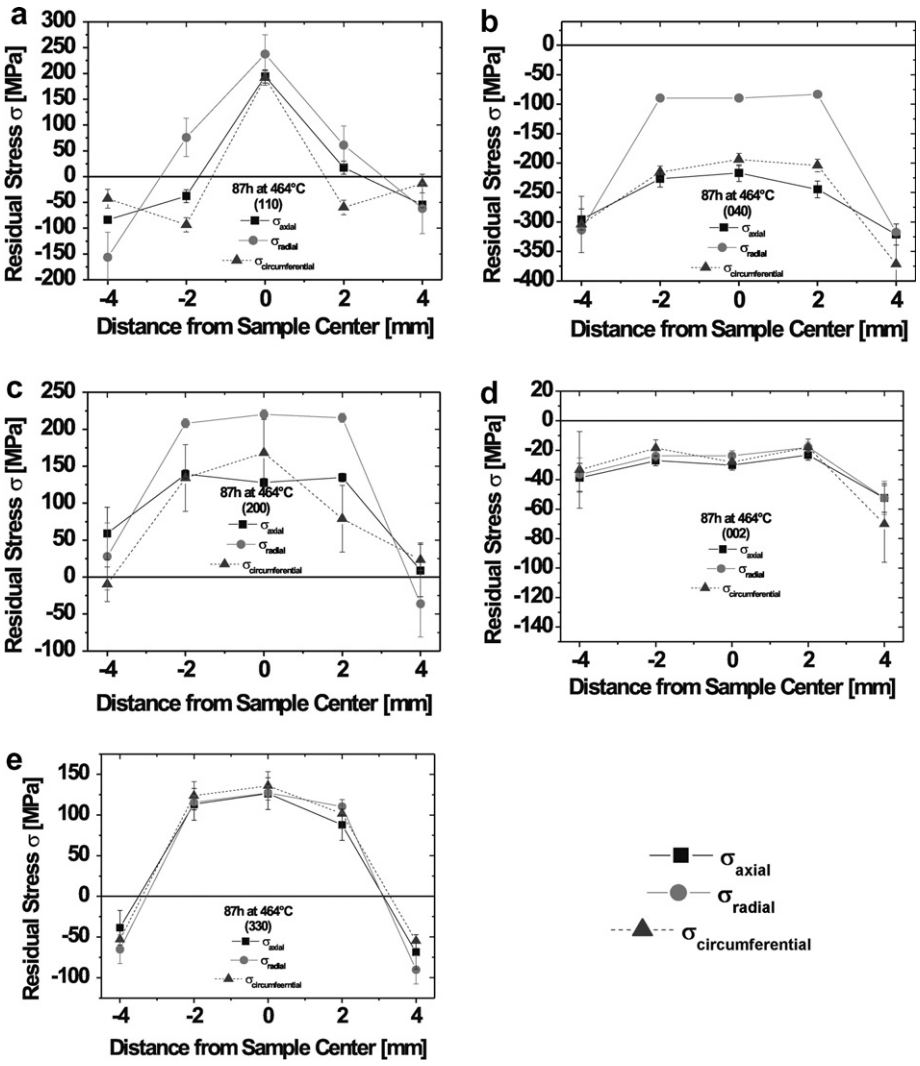

Fig. 9. Residual stress profiles across the sample heat treated 87 h at 464 °C for different (hkl) reflections in the axial, radial and circumferential sample directions: (a) (110), (b) (040), (c) (200), (d) (002), (e) (330).

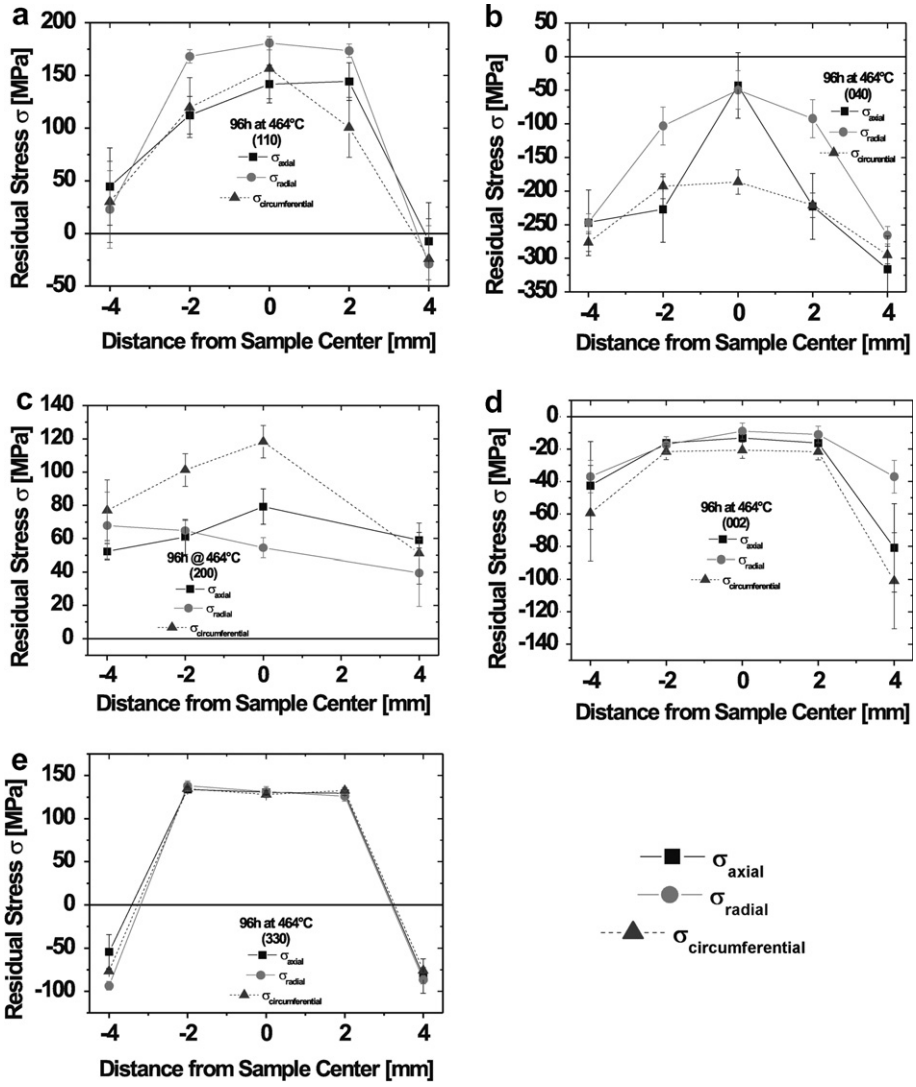

Fig. 10. Residual stress profiles across the sample heat treated 96 h at 464 °C for different (hkl) reflections in the axial, radial and circumferential sample directions: (a) (110), (b) (040), (c) (200), (d) (002), (e) (330).

residual stress state in the crystallites appears to be hydrostatic in the volume elements in the bulk of the samples as well as in the volume elements containing the near-surface zone.

The absolute values of the residual stresses determined in the three gauge volumes containing only crystallites from the bulk of the samples are very similar. The same holds for the stress values obtained in the gauge volumes near the edges of the samples. However, the average phase specific residual stress values obtained in the gauge volumes in the bulk appear to be different from those obtained in the gauge volumes at the edges of the sample for some of the reflections analyzed.

A comparison of the residual stress values obtained for different reflections in the gauge volumes within the bulk of the samples reveals that the sign and the magnitude of the residual stress values depend on the reflection used for residual stress analyses. The dependence of the residual stress values on the reflection is similar for the two samples (compare e.g. the phase specific residual stress values in the crystallites obtained for the 002 and 330 reflections).

Table 1
Near-surface residual stresses for different (hkl)-directions experimentally determined by the $\sin^2\psi$ technique, (hkl)-dependent thermal expansion mismatches and calculated residual stresses according to the modified Selsing model, Eq. (5)

(hkl)	$\sigma_{hkl}^{\sin 2\psi}$ (MPa) 96 h at 464 °C	$\Delta\alpha = \alpha_C^{hkl} - \alpha_g$ (10^{-6} °C)	$\sigma_{calc.}$ (MPa)
110	–	7.2	230
040	–	−7.5	−240
200	−56 ± 9	4.2	134
002	−71 ± 6	−4.5	−144
330	−53 ± 6	3.2	102
113	−26 ± 8	0.5	16
281	−54 ± 10	0.8	26
0100	−35 ± 15	−6.0	−192
370	−52 ± 6	1.3	−42

The phase specific stresses in the near-surface $Li_2Si_2O_5$ crystallites of the sample heat treated for 96 h at 464 °C were also determined by the $\sin^2\psi$-technique using medium energy (8.05 keV) synchrotron radiation. The residual stress values determined are compressive for all reflections investigated. The average phase specific stress value obtained is −50 MPa and most of the phase specific residual stress values determined on different reflection are within a standard deviation of 15 MPa (Table 1).

5. Discussion

5.1. Microstructure

The formation of a fully crystallized surface layer has been already observed in glasses after heat treatments above T_g, see e.g. [27]. Concurrent nucleation of the metastable LS and the stable LS_2 phases takes place in $Li_2O \cdot 2SiO_2$ glasses exclusively in the early stages of crystallization. In case of heat treatments at 454 °C, significant fractions of LS are encountered only for heat treatments of less than 25 h. After about 100 h, less than 20% of the crystallized volume fraction corresponds to the metastable phase LS [28,29]. Therefore, due to the long annealing times of 86 h and 96 h at 464 °C, LS_2 ($Li_2Si_2O_5$) would be expected to be predominant. This was confirmed by our XRD analyses using the Rietveld method. Nevertheless, the presence of small amounts of LS cannot be excluded, since very small volume fractions (<5%) might be below the detection limit.

The $Li_2Si_2O_5$ crystals grow with a preferential orientation from the external surface towards the bulk of the sample. The weak (0 0 2) fiber texture obtained in the surface layer of both samples corresponds to a certain preferred orientation of the orthorhombic c-axis perpendicular to the sample surface. The same fiber texture was encountered with considerably higher strength in lithium silicate glass–ceramics prepared in a temperature gradient [32]. The crystallographic texture is accompanied by a morphological texture, i.e. the direction of the c-axis coincides with the direction of largest elongation of the needle-shaped crystals (Fig. 3).

5.2. Residual stresses

Generally, only the crystalline phase may be assessed by residual stress analyses using diffraction methods. Only recently, stresses in amorphous materials have been determined using synchrotron radiation [37]. However, the new method proposed in [37] has only been proven for the characterization of load stress distributions, where a determination of the stress-free lattice spacing is not necessary.

Hence, residual stresses analyzed by synchrotron X-ray diffraction both in the near-surface zone and the bulk of the samples are phase specific stresses of the $Li_2Si_2O_5$ crystals. Due to the annealing process after glass fabrication and the slow cooling rates after the heat treatments, temperature and, consequently, density gradients across the samples were quite small. Thus, macro residual stresses in the samples are presumably negligible. Furthermore, elastic micro stresses due to differences in density between glass and crystal are supposed to relax, since the crystallites are nucleated above T_g.

Therefore, the stresses in the crystals within the bulk are mainly due to differences in the thermal expansion coefficient and the elastic properties of the amorphous matrix and the single crystallites. Due to the very small crystalline volume fraction in the bulk, the average distance between bulk crystals is 2 μm. Therefore, the distance between neighboring crystallites can be considered large compared to the typical crystallite diameter (0.3 μm). This leads to an isolation of individual crystals within the amorphous bulk material and, consequently, superposition of stress fields does not occur for most crystals.

Thus, in order to estimate the phase specific residual stresses caused by the thermal expansion mismatch, each crystallite will be considered to be surrounded by an infinitely large matrix. The best-known model for treating the so-called inclusion problem is the Eshelby model [33–35]. Since the tensors describing the elastic and thermal material properties are not known for the Li_2O–SiO_2 system, we applied as a first approximation a simplified inclusion model developed by Selsing [36] for assessing the residual stresses within the crystalline particles. According to [36] the micro residual stresses in the matrix close to spherical and isotropic inclusions can be described by

$$\sigma_r = -P(R/x)^3 \tag{4}$$

$$P = \Delta\alpha\Delta T/K_e \tag{5}$$

σ_r is the radial stress, P is the hydrostatic thermal stress acting within the inclusion, R is the inclusion radius, x is the distance from the center of the inclusion, $\Delta\alpha = \alpha_i - \alpha_m$ is the thermal expansion mismatch, ΔT is the temperature difference between T_g and the ambient temperature.

$$K_e = [(1+\nu_m)/2E_m + (1-2\nu_i)/E_i] \tag{6}$$

ν and E are Poisson's ratio and Young's modulus, respectively. The subscripts m and i refer to matrix and inclusion, respectively. Eqs. 4,5 hold for isotropic systems under the condition that the stress fields around each inclusion do not overlap with their neighboring stress fields.

The macro residual stresses σ^I due to thermal tempering, which were initially assumed as negligible, can be reassessed for each gauge volume analyzed by HESD using the mechanical equilibrium condition. Thus, it follows for sufficiently large sample volumes in polyphase glass–ceramics that:

$$\sum_i f^i \cdot \sigma_i^{II} = 0 \tag{7}$$

$$\sigma_{i,hkl}^{II} = \sigma_{i,hkl}^{experimental} - \sigma^I \tag{8}$$

where i refers to a certain phase constituent i, σ_i^{II} corresponds to the averaged phase specific micro residual stress,

$\sigma^{II}_{i,hkl}$ is the phase specific micro residual stress in the lattice plane (hkl) and $\sigma^{experimental}_{i,hkl}$ is the phase specific residual stress experimentally determined in the lattice plane (hkl). Replacing σ^{II}_i in Eq. (7) by Eq. (8), the macro residual stresses σ^{I} within each gauge volume can be derived from

$$\sigma^{I} = f^{C} \cdot \frac{1}{n} \Sigma_{n(hkl)} \sigma^{experimental}_{crystal,hkl} + (1 - f^{C}) \cdot \bar{\sigma}^{II}_{glass} \quad (9)$$

The mean micro residual stress in the amorphous matrix $\bar{\sigma}^{II}_{glass}$, which is unknown in Eq. (9), can be estimated using the following equilibrium condition applied to a sample cross-section:

$$\bar{\sigma}^{II}_{BC} \cdot A_{BC} + \bar{\sigma}^{II}_{SL} \cdot A_{SL} + \bar{\sigma}^{II}_{glass} \cdot (A_{sample} - (A_{BC} + A_{SL})) = 0 \quad (10)$$

$\bar{\sigma}^{II}_{BC}$ and $\bar{\sigma}^{II}_{SL}$ are the mean thermal micro residual stresses in the bulk crystallites and the surface layer, respectively. A_{sample}, A_{SL}, and A_{BC} represent the area of sample cross-section and the areas covered by the surface layer and bulk crystals on the cross-section, respectively.

Due to the very low volume fraction of bulk crystallites, $\bar{\sigma}^{II}_{BC}$ is the same for both samples and described by Eq. (5) ($\bar{\sigma}_{BC} = p$). On the other hand, $\bar{\sigma}_{SC}$ cannot be simply estimated using Selsing's model (Eq. (5)), which assumes a particle embedded in an infinitely large matrix. In contrast to $\bar{\sigma}^{II}_{BC}$, $\bar{\sigma}^{II}_{SL}$ is different for each sample due to the different thicknesses of the surface layers formed after 87 h and 96 h heat treatment, about 2 μm and 3.5 μm, respectively. Thus, $\bar{\sigma}^{II}_{SL}$ was evaluated using an elastic model for a layered composite [38–40] accounting for a thermal expansion mismatch ($\Delta\alpha$) with respect to the isotropic thermal expansion coefficient of the glass–ceramic composite $\bar{\alpha}$ and for the thicknesses of the surface layer and bulk material:

$$\bar{\sigma}^{II}_{SL} = \frac{\frac{E_C}{1-\nu_C}(\bar{\alpha}_C - \bar{\alpha}) \cdot \Delta T}{1 + \frac{t_{SL}}{t_{BM}} \frac{E_C}{E_{BM}} \frac{1-\nu_{BM}}{1-\nu_C}} \quad (11)$$

$$\bar{\alpha} = \frac{f^{C}\overline{E}^{C}\bar{\alpha}_C + f^{glass}\overline{E}^{glass}\alpha_{glass}}{f^{C}\overline{E}^{C} + f^{glass}\overline{E}^{glass}} \quad (12)$$

E_C, E_{BM} and ν_C, ν_{BM} represent the elastic properties of the fully crystallized surface layer and the bulk material, respectively, t_{SL}, t_{BM} are the thicknesses of the surface layer and the bulk material, f^{C} and f^{glass} are the volume fractions of crystallites and glassy phase, $\overline{E}^{C} = \frac{E^{C}}{1-\nu^{C}}$ and $\overline{E}^{glass} = \frac{E^{glass}}{1-\nu^{glass}}$.

For estimating the average thermal micro stresses in the bulk crystals $\bar{\sigma}^{II}_{BC}$ and surface layer $\bar{\sigma}^{II}_{SL}$ using Eqs. (5), (11) and (12) the following data were used:

- $\Delta T = 425$ °C (a temperature range from T_g down to room temperature, where the matrix plasticity is negligible).
- $\alpha_{glass} = 12.8 \times 10^{-6}$ °C^{-1}, $\bar{\alpha}_C = 10.8 \times 10^{-6}$ °C^{-1} (see [12]).
- $\nu_m = 0.23$; $\nu_i = 0.19$; $E_m = 7.5 \times 10^4$ MPa; $E_i = 12.2 \times 10^4$ MPa (due to the lack of single crystal data, average values for ν_i and E_i of $Li_2Si_2O_5$ polycrystals were employed).

From Eq.(12) the isotropic thermal expansion coefficients of the glass–ceramics, $\bar{\alpha}_{87h} = 12.7 \times 10^{-6}$ °C^{-1} and $\bar{\alpha}_{96\,h} = 12.6 \times 10^{-6}$ °C^{-1}, were determined. Thus, it was demonstrated by Eq. (5) and (11), respectively, that is about −64 MPa and $\bar{\sigma}^{II}_{SL}$ is −120 MPa for 87 h and −114 MPa for 96 h heat treatment. These calculated values for $\bar{\sigma}^{II}_{SL}$ are twice as high as the experimental values obtained from the near-surface zone using the $\sin^2\psi$ technique, which represented also an average over the crystallized surface layer and bulk crystallites. However, if the 40 μm penetration depth of the synchrotron X-rays (at 8.05 keV) and the 3.5 μm thick surface layer after 96 h heat treatment are taken into account, we can estimate the average micro residual stresses in the crystals within the near-surface volume analyzed by medium energy synchrotron X-rays. Indeed, the calculations reveal an average residual stress of −67 MPa in the LS_2-crystals within the gauge volume covered by the medium energy synchrotron X-rays, which corresponds to our average experimental values obtained by the $\sin^2\psi$ technique (−50 ± 15 MPa).

After determining $\bar{\sigma}^{II}_{BC}$ and $\bar{\sigma}^{II}_{SL}$, the average micro stresses in the amorphous matrix $\bar{\sigma}^{II}_{glass}$ can be assessed using Eq. (10). Due to the very low crystallized volume fraction (4–7%) in the bulk and the small volume of the fully crystallized surface layer, the mean residual stresses in the amorphous matrix $\bar{\sigma}^{II}_{glass}$ are very small tensile stresses. According to Eq. (10), $\bar{\sigma}^{II}_{glass}$ ~3 MPa and 5 MPa for the samples heat treated 87 and 96 h, respectively. $\bar{\sigma}^{II}_{glass}$, as an average value, is therefore not relevant with respect to the mechanical properties of a glass–ceramic, since the micro residual stresses in the glass phase σ^{II}_{glass} vary locally and their values reach the opposite value of the micro residual stresses acting within the crystallites at the crystal/glass interfaces.

After estimating $\bar{\sigma}^{II}_{glass}$, the macro residual stresses σ^{I} within each gauge volume analyzed using HESR can be reassessed. Eq. (9) reveals average macro residual stresses of −1 MPa and +3 MPa for the external sample surface and the bulk, respectively, and confirms that the residual macro stresses induced by inhomogeneous temperature fields during sample cooling are insignificant in the present study.

However, the $Li_2Si_2O_5$ crystals show a crystallographic anisotropy of thermal expansion due to their orthorhombic structure [12]. In addition, it is assumed that the spherical crystallites are embedded in an infinitely large matrix, since the crystalline volume fraction in the bulk is very low. Thus, we applied Selsing's model once again in order to estimate the local anisotropy of the residual micro stresses. Hence, the average thermal expansion coefficient of the crystalline phase $\bar{\alpha}_C$ was replaced in Eq. (5) by the thermal expansion coefficients along each different crystallographic (hkl)-direction α^{hkl}_C [12]. The results of these calculations reveal the stresses in the crystals caused by the difference of their thermal expansion along each (hkl) direction (Table 1). A comparison of the calculated stress values obtained for different (hkl) directions shows that depending on the

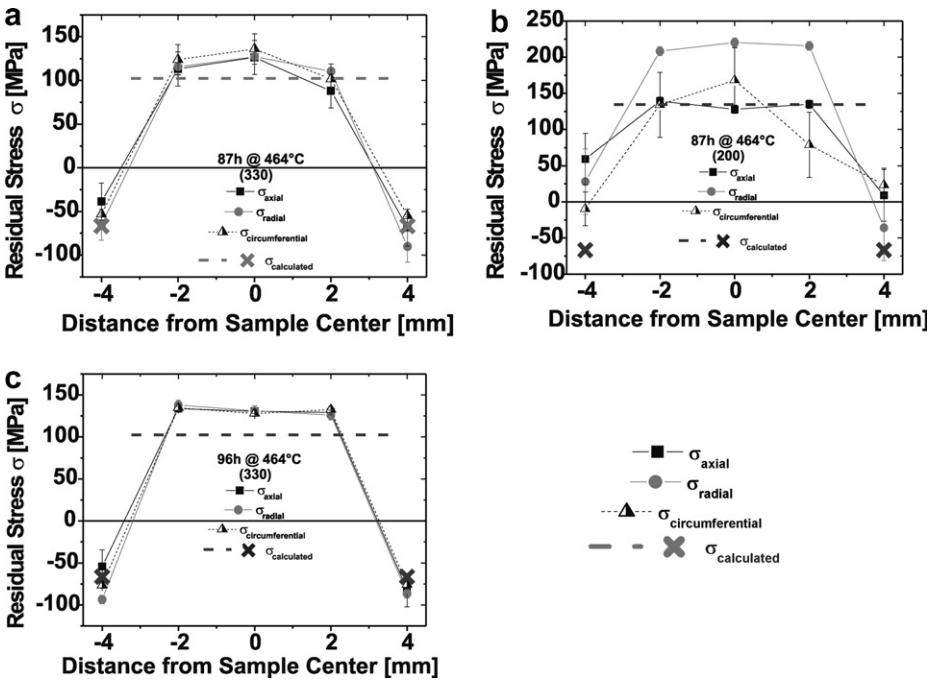

Fig. 11. Comparison between experimental residual stresses in the axial, radial and circumferential sample directions and calculated residual stresses according to Eqs. (5) and (11).

crystallographic direction the thermally induced stresses in the particles may be tensile as well as compressive and that their magnitudes differ by up to a factor of two.

The dependence of the residual stresses on the crystallographic orientation is visible also in the phase specific residual stress values determined by HESR in the bulk using different reflections (hkl). A comparison of the experimentally determined and the calculated residual stress values for different reflections (Fig. 11, the calculated stress values for the bulk are indicated by a dashed line and by a cross for the surface zone) in the bulk and the surface of the samples reveals in general a good agreement. In the bulk tensile residual stresses arise along those (hkl) directions, where the thermal expansion coefficient α_C^{hkl} is higher than the thermal expansion coefficient of the glassy matrix α_{glass}, while compressive residual stresses are formed if $\alpha_C^{hkl} < \alpha_{glass}$. In the near-surface zone an average compression exists, since $\bar{\alpha}_C < \alpha_{glass}$.

Regarding the application of $Li_2O \cdot 2SiO_2$ glass–ceramics, the fact that compressive residual stresses of about 120 MPa are generated at the external surfaces, because $\bar{\alpha}_C < \alpha_{glass}$, may increase the lifetime of components operating at RT, since compressive stresses are beneficial with respect to crack growth under tensile loading. This fact could explain the relatively high fracture strength of some commercial $Li_2O \cdot 2SiO_2$ glass–ceramics.

6. Summary and conclusions

The microstructure and its influence on the formation of residual stresses were studied in partially crystallized $Li_2O \cdot 2SiO_2$ glasses. After heat treatments of 87 h and 96 h at 464 °C, only the stable $Li_2Si_2O_5$ phase with an orthorhombic crystal structure was observed. Crystallization takes place homogeneously in the bulk material with the formation of low crystalline volume fractions (4–7%) of nearly spherical crystals. The typical crystallite size in the bulk microstructure is below 0.5 μm. At the external surface nucleation and crystallization occur heterogeneously and a very thin fully crystallized surface layer of about 2.0–3.5 μm after 87–96 h heat treatment is formed. This surface layer grows spontaneously with a weak preferential orientation of the orthorhombic c-axis perpendicular to the external surface.

The residual stresses of the crystalline $Li_2Si_2O_5$-phase in the bulk of partially crystallized $Li_2O \cdot 2SiO_2$ glasses are locally anisotropic for small crystallized volume fractions. The anisotropy of the residual stresses in these glass–ceramics arise from the crystal structure of the crystalline phase formed, which may cause a crystallographic dependence of the thermal expansion coefficient and elastic constants. With increasing degree of crystallization (particularly in the near-surface zone), there is a trend to develop isotropic residual stresses, which do not depend on the lattice planes. Their sign is given by the mean thermal expansion mismatch of the system.

The method presented here, which combines the model for isotropic particles developed by Selsing with a thermal elastic approximation for thin films, may be useful to predict the spatial residual stress distribution in other glass–ceramic samples, even in case of thermal and elastic anisotropy. From a technological point of view, compres-

sive stresses arising in the near-surface zone offer an interesting alternative to increase the mechanical performance of glass–ceramic components. To the best of our knowledge, residual stresses in embedded crystals were measured for the first time directly in the interior of a glass–ceramic without the need to eliminate the crystallized surface layer.

Acknowledgments

This research was supported by ADEMAT Network, Alfa II Project No. II-0240-B1-AT-RT-CT and by the Contract RII3-CT-2004-506008 (IA-SFS) of the European Commission. ESRF and HASYLAB are kindly acknowledged for providing synchrotron beamtimes. Professor Dr W. Reimers, Technical University Berlin, is acknowledged for many fruitful discussions.

References

[1] P.W. McMilan, Glass–Ceramics, Academic, London, 1964 (Chapter 3).
[2] D.J. Green, J. Am. Ceram. Soc. 64 (1981) 138.
[3] J.F. Ganghoffer, Mech. Time-Depend. Mater. 4 (2000) 359.
[4] C.C. Aydiner, E. Ustündag, M.B. Prime, A. Peker, J. Non-Cryst. Solids 316 (2003) 82.
[5] C.C. Aydiner, E. Ustündag, Mech. Mat. 37 (2005) 201.
[6] H. Fischer, M. Hemelik, R. Telle, R. Marx, Dental Mater. 21 (2005) 671.
[7] J. Möller, J. Schmelzer, I. Gutzow, J. Non-Cryst. Solids 240 (1998) 131.
[8] J.W.P. Schmelzer, O.V. Potapov, V.M. Fokin, R. Müller, S. Reinsch, J. Non-Cryst. Solids 333 (2004) 150.
[9] R.M. Fulrath, J. Am. Ceram. Soc. 42 (9) (1959) 423.
[10] L.S. Zevin, E.A. Levi, Z.G. Bessmertnaya, Neorg. Mater. 13 (10) (1977) 1880.
[11] E.D. Zanotto, M.L.G. Leite, J. Non-Cryst. Solids 202 (1996) 145.
[12] V.R. Mastelaro, E.D. Zanotto, J. Non-Cryst. Solids 247 (1999) 79.
[13] V.F. Libeau, Acta Crystallogr. 14 (1961) 389.
[14] V.R. Mastelaro, E.D. Zanotto, J. Non-Cryst. Solids 194 (1996) 297.
[15] M.E. Fitzpatrick, A. Lodini, Analysis of Residual Stress by Diffraction using Neutron and Synchrotron Radiation, Taylor & Francis, London, 2003.
[16] V. Hauk, Structural and Residual Stress Analysis by Nondestructive Methods, Elsevier, Amsterdam, 1997.
[17] I.C. Noyan, Adv. X-ray Anal. 28 (1985) 281.
[18] E. Macherauch, P. Müller, Z. f. Angew. Phys. 13 (1961) 305.
[19] I.C. Noyan, J.B. Cohen, Residual Stress: Measurement by Diffraction and Interpretation, Springer, New York, 1987.
[20] Y.D. Huang, L. Froyen, e-Journal of Nondestructive Testing; www.ndt.net, 6 (5) 2001.
[21] L. Lutterotti, P. Scardi, P. Maistrelli, J. Appl. Cryst. 23 (1990) 246.
[22] L. Lutterotti, S. Gialanella, Acta Mater. 46 (1998) 101.
[23] P. Scardi, L. Lutterotti, P. Maistrelli, Powder Diffr. 9 (1994) 180.
[24] P. Sahu, M. De, S. Kajiwara, Mat. Sci. Eng. A 333 (2002) 10.
[25] P. Sahu, M. De, S. Kajiwara, J. Alloys Compd. 346 (2002) 158.
[26] P.F. James, Y. Iqbal, U.S. Jais, S. Jordery, W.E. Lee, J. Non-Cryst. Solids 219 (1997) 17.
[27] J. Schmelzer, J. Möller, I. Gutzow, R. Pascova, R. Müller, W. Pannhorst, J. Non-Cryst. Solids 183 (1995) 215.
[28] E.D. Zanotto, J. Non-Cryst. Solids 219 (1997) 42.
[29] P.C. Soares Jr., E.D. Zanotto, V.M. Fokin, H. Jain, J. Non-Cryst. Solids 331 (2003) 217.
[30] B.H.W.S. De Jong, P.G.G. Slaats, H.T.J. Supèr, N. Veldman, A.L. Spek, J. Non-Cryst. Solids 176 (1994) 164.
[31] K.F. Hesse, Acta Crystallogr. B 33 (1977) 901.
[32] K. Engel, G.H. Frischat, J. Non-Cryst. Solids 196 (1996) 339.
[33] J.D. Eshelby, Proc. Roy. Soc. (London) A241 (1957) 376.
[34] P.J. Withers, in: Measurement of Residual and Applied Stress Using Neutron Diffraction, Kluwer Academic, Dordrecht, Boston, London, 1992, p. 421.
[35] P.J. Withers, W.M. Stobbs, O.B. Pedersen, Acta Metall. 37 (1989) 3061.
[36] J. Selsing, J. Am. Ceram. Soc. 44 (1961) 419.
[37] H.F. Poulsen, J.A. Wert, J. Neuefeind, V. Honkimäki, M. Daymond, Nature Mater. 4 (2005) 33.
[38] H. Behnken, Mikrospannungen in vielkristallinen und heterogenen Werkstoffen, Habilitationsschrift, ISSN 0945-1056, RWTH Aachen, 2003.
[39] A.M. Huntz, S. Daghigh, A. Piano, J.L. Lebrun, Mat. Sci. Eng. A A248 (1998) 44.
[40] M. Schulte, M. Schütze, Oxid. Met. 51 (112) (1999) 55.